Journal of Materials Science: Materials in Electronics (2019) 30:4831–4841
https://doi.org/10.1007/s10854-019-00777-4

# Tensile characteristics of Sn–5wt%Sb–1.5wt%Ag reinforced by nano-sized ZnO particles

**M. M. Mansour[1] · A. Fawzy[1] · L. A. Wahab[2] · G. Saad[1]**

Received: 29 November 2018 / Accepted: 19 January 2019 / Published online: 12 February 2019
© Springer Science+Business Media, LLC, part of Springer Nature 2019

**Abstract**

In this study the impact of adding 0.3 wt% ZnO nano-sized particles into Sn–5wt%Sb–1.5wt%Ag (SSA) lead free solder (LFS) was investigated for microstructure, thermal and tensile stress strain characteristics. The microstructure of both the plain and composite LFS was examined by utilizing the optical microscopy (OM), scanning electron microscopy (SEM), energy dispersive X-ray spectroscopy (EDS) and X-ray diffraction (XRD). The addition of ZnOnano-sized particles drastically changed the microstructure and improved the tensile response of SSA LFS. The microstructure investigations showed the formation of the intermetallic compounds (IMCs) $Ag_3Sn$ and SnSb. Sizes of the formed IMCs were found finer in the ZnO-contained solder. In this work the alloy under investigation exhibited better tensile response with the refined IMC particle. Thermal analysis of the composite solder revealed a slight decrease (0.08 °C) in freezing point, low pasty range (6.55 °C) and low degree of undercooling (3.39 °C). These findings are expected to supply a correct guideline and reference in producing of electronic packages.

## 1 Introduction

Historically, for a protracted time Sn–Pb solder alloy has been used because of its superior wettability, good performance, moderate melting temperature (183 °C) and low price in trendy electronic packaging. In recent years, Pb-free solder (LFS) alloys are rapidly replaced the traditional eutectic SnPb solder in the electronics industry and using of lead has been restricted. Since 2006 the international legislations forestall exploitation of lead (Pb) within the industrial product because of its serious environmental and toxicological considerations [1, 2]. Moreover, miniaturization and diversification is that the current trend of the electronic elements. These electronic elements demands reliable solder joint to keep up the performance and overall product reliability. It has been considered as a promising candidate to substitute the Sn–Pb solder alloys. So, over the past years, most researchers are targeted on Sn–Ag, Sn–Cu, Sn–Zn and Sn–Sb alloys as doable different LFS [2–5].

✉ A. Fawzy
afawzy1955@yahoo.com

[1] Department of Physics, Faculty of Education, Ain Shams University, Cairo, Egypt

[2] Department of Physics, National Centre for Radiation Research and Technology, Nasr City, Cairo, Egypt

Notably, Sn–5wt%Sb LFS alloy was introduced as an interest group attributed to its smart mechanical properties [6]. Effect of Ag on microstructure, thermal and creep properties of Sn–5Sb-based lead-free solder alloy was investigated. From microstructure examination, the cuboids SnSb intermetallic compound is precipitated within the β-Sn matrix in the Sn–5Sb-based lead-free solder alloy. The ternary alloys Sn–5Sb–3.5Ag exhibited additional $Ag_3Sn$ intermetallic compound IMC.

Although addition of Ag decreased the melting point of Sn–5Sb from 240 to 216 °C but high content of Ag decreased the toughness of interfacial intermetallic layer of Ag3Sn. New generation LFSs are being designed to enhance the toughness of interfacial intermetallic layer (IML). The outcome has been the development and implementation of low Ag alloys to improve the mechanical strength of solder joints, especially under dynamic loading conditions. There is however a concern that these low Ag alloys will exhibit low mechanical response compared with those of high Ag content.

Nowadays, to supply high stability in microstructure and higher mechanical response with respect to traditional solders, LFSs were integrated with nano-sized, nonreacting, noncoarsening compound dispersoids which are known as reinforcements, it seems to be like vitamins to LFSs. So, in order to improve physical and mechanical properties of

LFS, some of these reinforcement particles are introduced into LFS alloys which is proposed as an effective method to elevate the reliability of solder joints. There are numerous publications introduced to improve physical and mechanical response of LFS; Gain et al. [7] studied SAC305-1wt% $TiO_2$ solder and found that its hardness increased as a result of $TiO_2$ addition. The presence of such reinforcement particles $Al_2O_3$ [8], $ZrO_3$, NiO [9] and $TiO_2$ [10] as nano-sized particles frequently reinforce the microstructure, modify thermal characteristics and enhance mechanical response of lead free solders. In a previous study Sn–1.7Sb–1.5Ag solder alloy bolstered with $Al_2O_3$ nanoparticles [11], decrease its minimum strain rate compared with that of the plain solder alloy at different testing conditions. This was attributed to the dispersive distribution of the nano-metric particles of $Al_2O_3$ within the composite solder.

Literature survey showed that restricted studies are reported to develop Sn–Sb–Ag LFS joints containing ZnO nano-sized particles. ZnO is predicted to have remarkable effect on the microstructure since it has no solubility in β-Sn matrix. Consequently, the aim of the present study is to look at the microstructure, thermal and mechanical behavior changes that have occurred after addition of ZnO nanoparticles.

### 1.1 Experimental procedure

ZnOnano-sized particles were selected as a reinforcement oxide attributable to its benefits which are: (i) it's density of (6.95 g/$cm^3$) that is almost about the density of Sn–5wt%Sb (7.53 g/$cm^3$), (ii) higher hardness compared with matrix of Sn–5Sb (iii) chemical stability and (iv) low price when put next to different nano-sized particles like $TiO_2$, $Y_2O_3$ and $ZrO_2$ [12].

Low Ag LFS, Sn–5.0wt%Sb–1.5wt%Ag (SSA plain), was prepared by melting Sn, Sb and Ag ingots of 99.99%. The composite SSA-0.3wt% ZnO solder was prepared by mechanical mixing of 0.3 wt% nano-sized ZnO particles into the liquid plain SSA LFS. After casting, remelting in a vacuum chamber at 400 °C was made to get a homogeneous composition. The two solder alloys in the form of rods were cold drawn into a wire of 1.0 mm diameter. A part of each alloy was cold-rolled into a sheet of 2 mm thick for microstructure investigations. Specimens with a gauge length of 50 mm were adapted for tensile testing. To stabilize the microstructure and removing the residual defects that created throughout the cold-drawing process, all specimens were heat-treated at a temperature of 130 °C for 30 min and then slowly cooled to room temperature (~25 °C) before tensile testing. For metallographic observations, both types of specimens were ready at the start by mounting in cold epoxy and polished until they became finely polished surfaces. The carved and highly polished surfaces of the solder samples were etched in a solution of 10% nitric acid, 10% acetic acid and 80% glycerin and then examined by optical microscope (OM). The surface morphology of the two types of samples was characterized by using field emission scanning microscopy (FESEM) SU8000 series equipped with energy dispersive X-ray analysis EDX. X-ray diffractometry [Philips diffractometer (40 kV)] with atomic number 29 Kσ radiation (λ = 0.15406 nm) was used for XRD measurements. XRD patterns were recorded within the 2θ vary of 20°–90°.

The melting temperature, pasty range and degree of undercooling were determined by the utilization of the differential scanning calorimetry (DSC) Shimadzu DSC-50. The measurements were performed at a heating rate of 10 °C/min and high purity chemical element gas taste heating chamber to avoid oxidization of samples.

Tensile testing was performed by straining at different strain rates ranged from $13 \times 10^{-5}$ to $4.4 \times 10^{-3}$ $s^{-1}$. Every specimen was stretched until fracture under the effect of different strain rates and testing temperatures.

## 2 Results and discussion

### 2.1 Thermal analysis

Pb-free solder ought to be developed to be used at appropriate melting temperature, pasty range and degree of undercooling with none degradation. Melting temperature of a metal is a vital characteristic property since it determines the utmost operative temperature of the system [13].The freezing point of the prepared plain and composite solders was accurately characterized by DSC thermograms. Figure 1a, b shows the endothermal peak and the energy-releasing peak as operating of temperature throughout the heating and cooling with a rate of 10 K/min. The solidification properties of solders are very important in the election of the temperature profile for obtaining good assembly. From this point of view the melting and solidification can be characterized from the diffraction scanning caliometer curve. The melting temperature range of the plain and composite solders was found to be 239.71 and 239.63 °C respectively (Table 1). This result was found similar to those obtained in different studies on Sn–Sb–Ag [6] and Sn–Sb–Cu LFS [14]. The slight decrease (0.08 °C) in freezing point of the SSA composite solder is often attributed to the effect of the nano metric ZnO particles on the variation in physical properties of grain boundary/interfacial characteristics. Another important thermal parameter is the pasty range. The pasty range is defined as the difference between the solidus (Ts) and liquidus ($T_\ell$) temperatures. For SSA plain solder and SSA composite solder, the pasty range was found to be lying within the range of 6.55 °C (Table 1), which is not up to those of the binary Sn–5wt%Sb (10 °C) and Sn–Pb (11.5 °C) solders [6, 12, 14].

**Table 1** Thermal characteristics of SSA plain and composite solder

| Alloy | $T_{end}$ | $T_{onset}$ | $T_m$ | Pasty range ($T_{end}$–$T_{onset}$) | $T_{endheating}$ | $T_{onset\ cooling}$ | under cooling |
|---|---|---|---|---|---|---|---|
| Sn–5%Sb–1.5%Ag | 241.38 | 234.90 | 239.71 | 6.48 | 227.27 | 225.64 | 1.73 |
| Composite Sn–5%Sb–1.5%Ag | 240.97 | 234.5 | 239.63 | 6.47 | 226.99 | 223.60 | 3.39 |

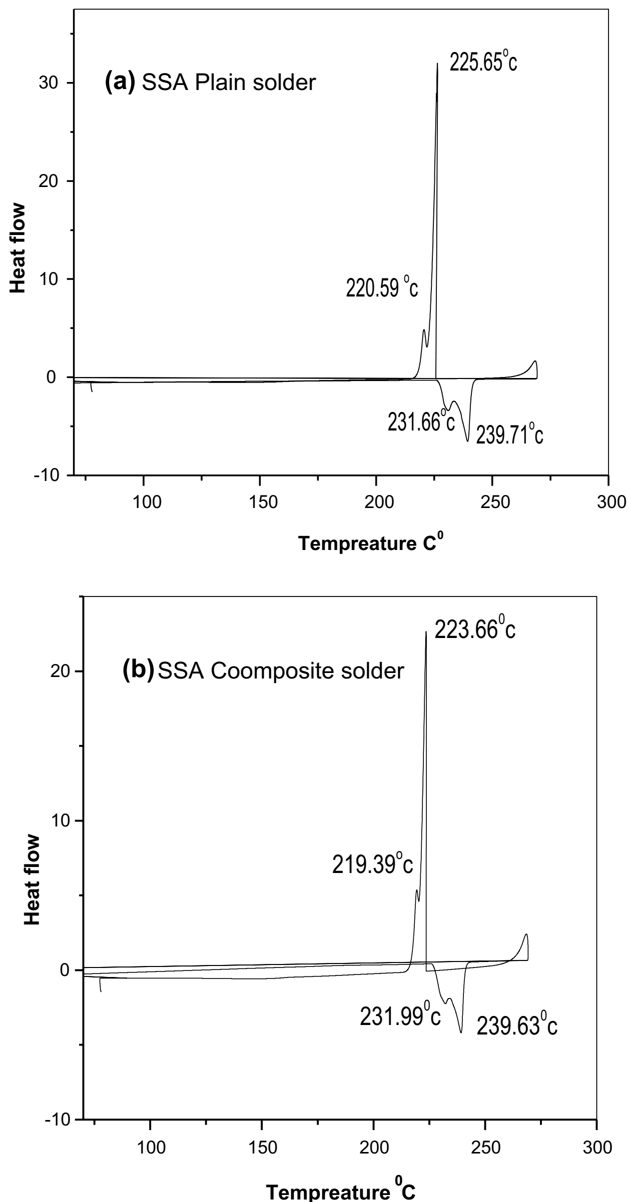


**Fig. 1** DSC curves for: **a** SSA plain and **b** SSA5 composite solder

Apparently, this small pasty range is probably going to avoid producing technical problems, like increasing the chance of the fillet lifting phenomena (separation of the solder from the copper pad), the tendency towards porousness and hot tearing contraction throughout activity. Also, the degree of undercooling is a vital thermal property since it is one of the decisive factors which have an effect on the coarsening of IMCs. The degree of undercooling is defined as the distinction between the $T_{onset}$ throughout heating and $T_{onset}$ throughout cooling, and relates to the problem of nucleating the solid innovate a liquid state. Consistent with this assumption, the degree of undercooling is often determined to be 1.73 °C for the plain and 3.39 °C for the composite LFS, respectively (Table 1). This value is smaller compared to that of the Sn–Pb solder alloy [15, 16] which can be added to the solder efficiency under investigation.

## 2.2 Microstructure analysis

XRD and TEM analyses are performed to scrutinize composition of the nano-metric ZnO particles used in the present work that was utilized in previous work on Sn–3.5Ag–0.5Cu in our science lab. The results seen in Fig. 2a, b showed a median size of nominally polyhedrons nano-sized ZnO particles with ~56 nm diameters [17–19]. X-ray investigation of the SSA plain and SSA-ZnO composite solders is illustrated by the diffraction patterns shown in Fig. 3a, b. This figure showed three kinds of phases: β-Sn, SnSb and $Ag_3Sn$ IMCs. The patterns of each solder are found to possess nearly identical features. Figure 4b, d shows optical and SEM micrographs of plain and composite solder, respectively. It shows a major decrease of the SnSb particle size and the β-Sn grains compared with plain samples shown in Fig. 4a, c.

According to the elemental composition map presented in Fig. 4e as well as Fig. 4b, d the chosen areas within the composite solder were found to contain Sn, Sb, Ag, Zn and O. Thus, it is already established that the matrix contains β-Sn, SnSb, $Ag_3Sn$ besides the ZnOnano-sized particles. The retarding effect of the ZnOnano-sized particles is analogous to that reported in different studies [12, 17–19]. This implies that addition of 0.3 wt% nano-sized ZnO to the plain SSA suppresses and controls the β-Sn grains, and IMC particles yielding dispersion of those IMCs among the Sn mixture forming fine network like microstructure with the β-Sn (Fig. 4b, d). This would have an effect on its physical and mechanical properties. To investigate the uniform distribution of the microstructure of this alloy, Electron Probe Micro-Analyzer (EPMA) analysis was performed on the surface of SSA-ZnO composite solder alloy (Fig. 4f). EPMA showed the uniform distribution of fine dot-like phases that

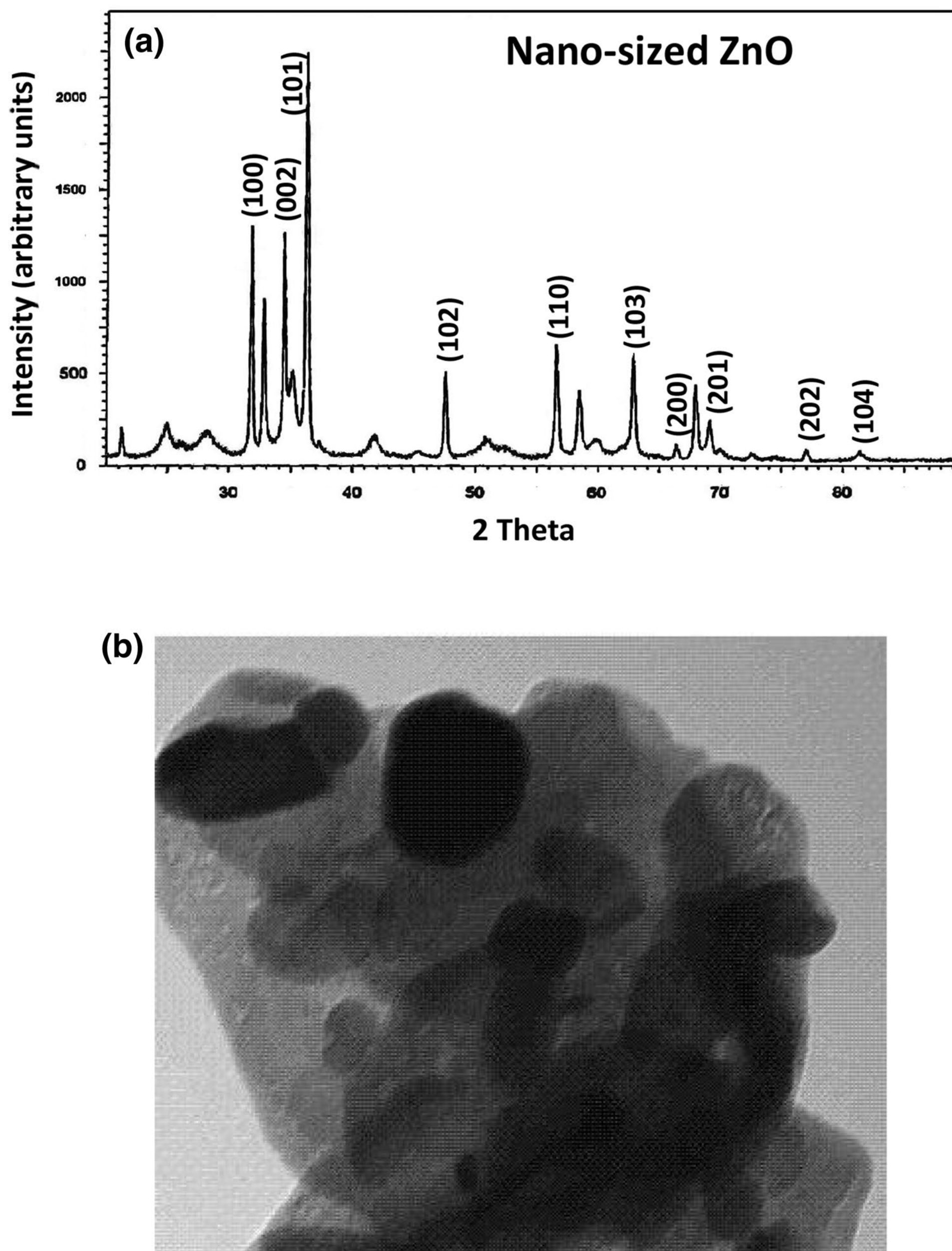


**Fig. 2** **a** XRD pattern of the nano-sized ZnO particles and **b** TEM of the nano-sized ZnO particle

is homogeneously distributed within the Sn-matrix and may effectively resist the movement of dislocations throughout mechanical deformation. They're necessary to understanding that the refinement of microstructure is expected to improve the tensile resistance of the solder under investigation.

## 2.3 Tensile tests

Systematic tensile tests performed for the two LFS alloys at the testing temperature 25 °C (room temperature, RT) under different strain rates are illustrated in Fig. 5a. Figure 5b represents a typical representative set of tensile stress strain curves for the plain SSA and SSA composite solder stretched with a strain rate of $1.2\times10^{-3}\ s^{-1}$ and tested at different temperatures in the range 298–383 K. In Figure 5a, b it is clear that increasing strain rate and/or decreasing testing temperature for both plain and composite LFS alloys resulted in shifting the levels of these curves towards higher values of stress.

The impact of nano-sized ZnO particles addition on the tensile properties is illustrated in Fig. 6a, b. Values of UTS and 0.2%YS for both solders tested at the same testing conditions show considerable increase with increasing $\dot{\varepsilon}$ and/or decreasing testing temperature. Therefore the composite LFS incorporates a profit to reinforce its mechanical strength that is in smart agreement with the prediction of the

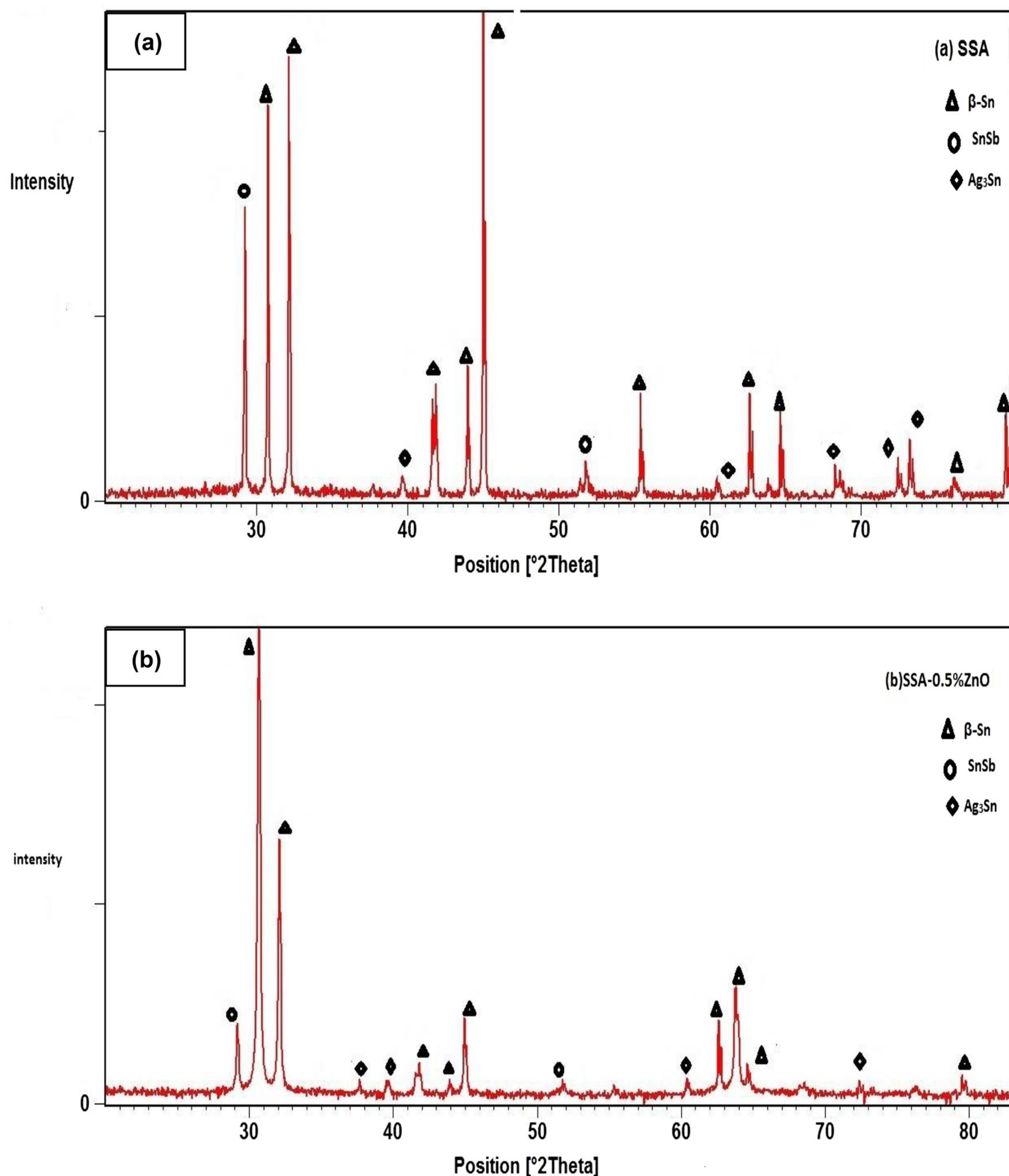


**Fig. 3** XRD patterns for **a** plain SSA and **b** SSA composite solder

classical theory of dispersion strengthening created by the addition of nano-sized ZnO particles. This result is credible once the UTS and 0.2YS of SSA composite LFS is usually attributed to the decrease of its grain sizes and refinement of each the β-Sn dendrites and also the IMCs Sn-Sb and $Ag_3Sn$ (Fig. 4b, d). Similar trends are also found within the Sn-based solder alloys in different studies [12, 14, 17–20]. They recommended that adding nano-sized ZnO particles exaggerated the strength of Sn-rich composite solders and attributed this behavior to the dispersion strengthening of the fine microstructure.

## 2.4 Effect of testing temperature and strain rate on the tensile stress–strain characteristics of SSA and SSA-ZnO solders

Figure 6a illustrates the dependence of 0.2%Ys on strain rate ($\dot{\varepsilon}$) for both the plain and composite solder at different

**Fig. 4** **a** Optical micrographs for the plain SSA, **b** optical micrographs for the plain SSA composite solder, **c** SEM for the SSA plain SSA solder, **d** SEM for the SSA composite solder and **e** EPMA for the SSA composite solder and **f** EDS for the composite SSA solder showing the elements contained in the composite solder

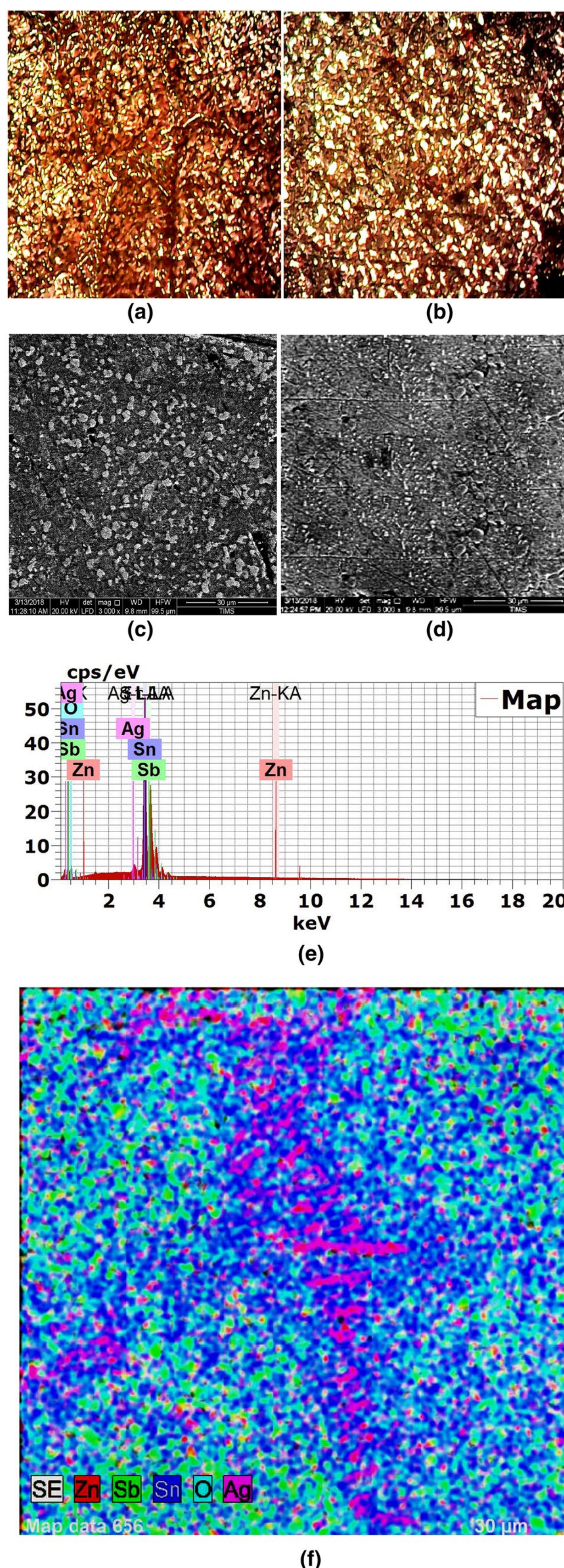


testing temperatures. Figure 6b the dependence of UTS of both solders under the testing conditions. The improvement of tensile properties as a result of increasing ε˙ may be attributed to the restricted time for the dislocation motion that makes dense promise dislocations and additional hardening effects as reported by Fawzy et al. [18, 19]. Obviously, the composite solder alloy has higher durability compared with the plain LFS at the same testing conditions.

The high strength levels obtained at 0.3 nano-sized ZnO particles addition imply that many doable reasons will contribute to the current strengthening mechanism like, the distribution of the finer: β-Sn, SnSb and $Ag_3Sn$ phases that act as pinning centers inhibiting the quality of the dislocations focused around grain boundaries [19, 20]. Moreover, additional dislocations are generated by totally different slippy planes and numerous orientations act as exhausting blockers, which increase the strength of the alloy.

The temperature dependence of the stress–strain characteristics 0.2%YS and UTS (Fig. 7a, b) could be explained with view to the dynamic recovery method. The superior durability of SSA composite solder as compared to the plain SSA solder could be attributed to refinement of the β-Sn grains and the refined SnSb and $Ag_3Sn$ IMCs IMCs (Fig. 4b, d). This refinement could also be attributed to the effect of the nano-sized ZnO particles coagulated on grain surfaces through the matrix during the solidification process. It was observed from the stress–strain curves of Fig. 5b that the overall elongation was found to change irregularly for each solder alloy. Many reasons exist for the plasticity sensitivity to testing temperatures: (i) these embody composition and heat treatment effects on the matrix and IMCs, (ii) the character of interfacial reaction between the IMCs and (iii) the soundness of the soft and exhausting IMCs within the alloy matrix [21].

### 2.5 Strengthening mechanisms in SSA-ZnO composite solder

The enhancement of the 0.2YS and UTS of SSA-ZnO composite solder alloy can be attributed to totally different strengthening mechanisms of the hardened reinforcement ZnOnano-sized particles in addition to the finer IMCs in β-Sn matrix. This strengthening behavior may be a result of one or more of the following factors:

(i) grain refinement [22]; (ii) formation of internal stress due to the difference in coefficient of thermal expansion

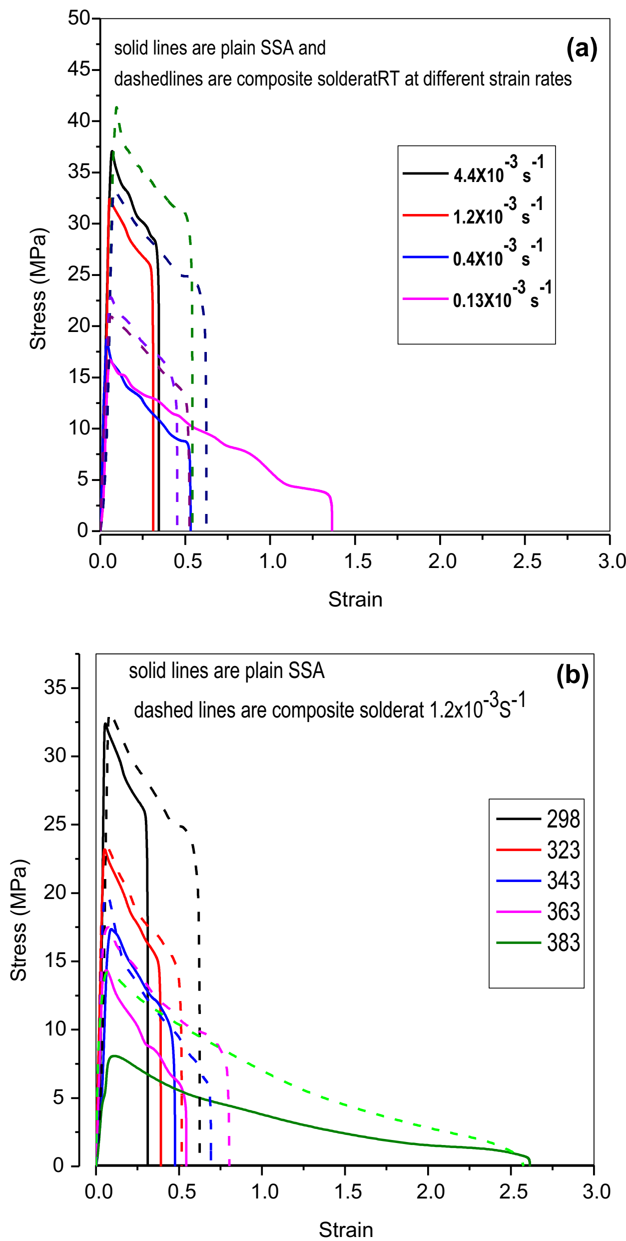


**Fig. 5** Comparative representative stress–strain curves showing: **a** the effect of strain rate and **b** the effect of temperature on the two solders stretched at a constant strain rate as indicated

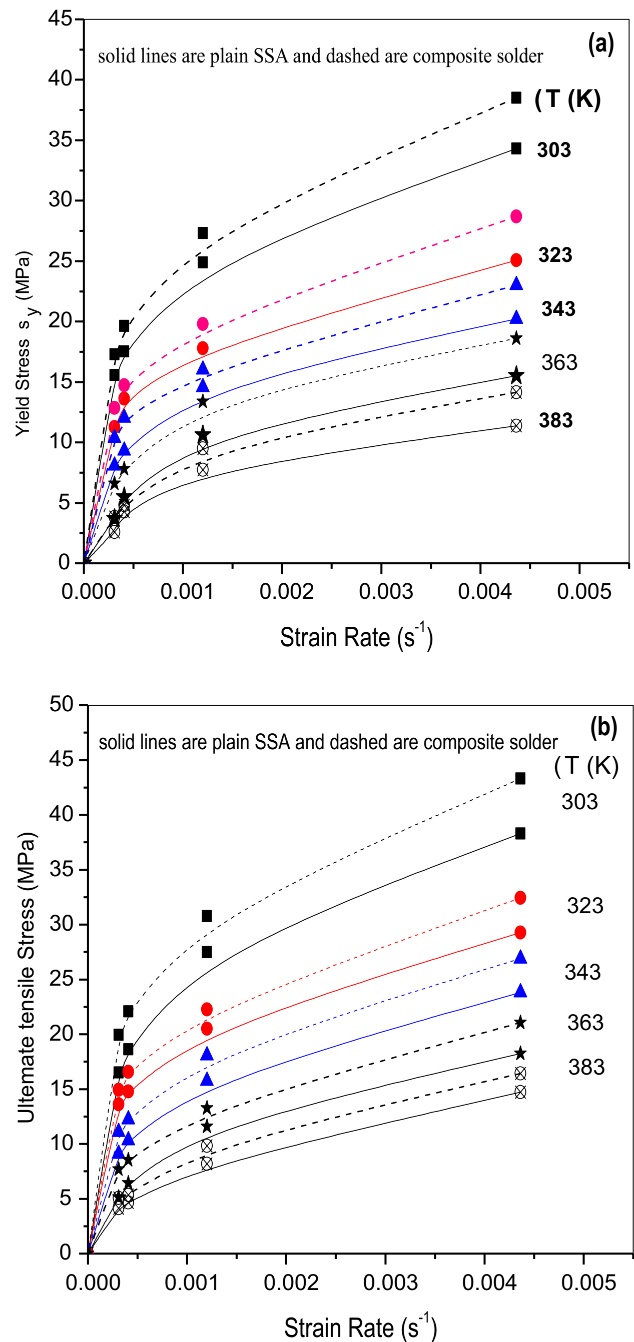


**Fig. 6** Strain rate dependence of: **a** yield stress, **b** ultimate tensile stress for the two solder alloys

(CTE) between the Sn matrix and nano-sized particles; (iii) Orowan strengthening mechanism; and (iv) adsorption of the nano-metric ZnO particles on the solidified grain surfaces through the matrix during solidification process [23–25].

### 2.5.1 The effect of particle size refinement

Grain size effect on tensile properties can be considered from two points of view; (i) in a matrix of small grain sizes, the grain boundaries may act as obstacles to dislocation motion leading to strengthening effect; (ii) It has been mentioned before (see Fig. 4b, d) that the presence of ZnOnano-sized particles act as pinners to the grain boundary migration

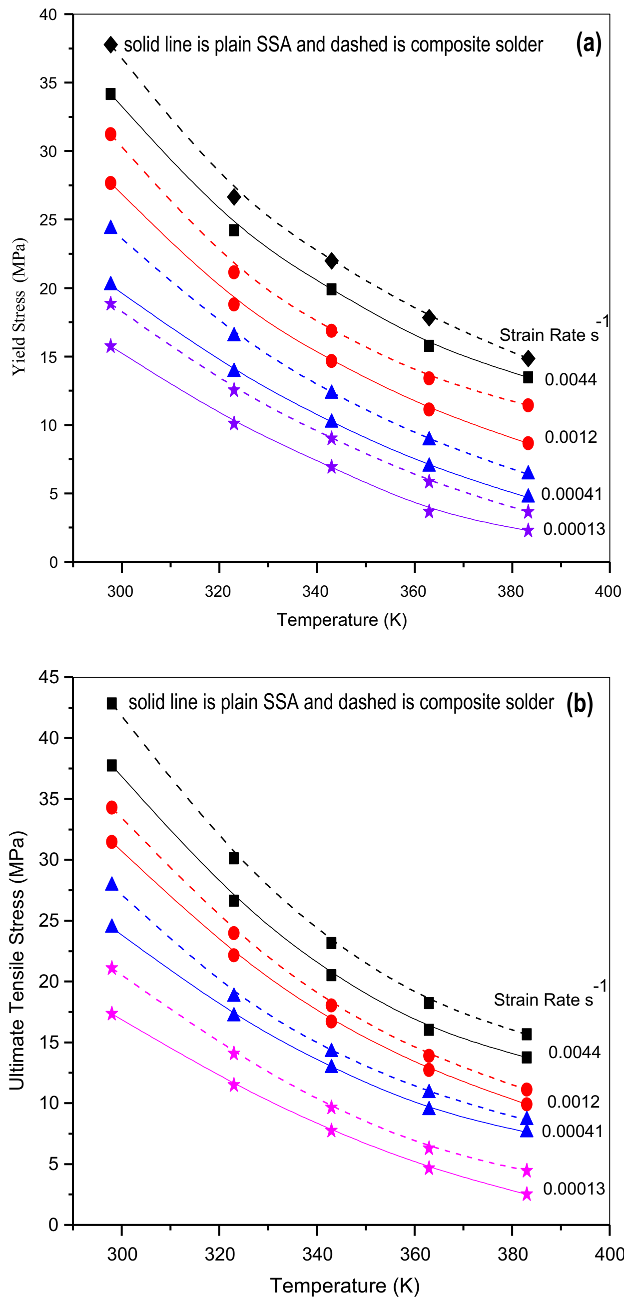


**Fig. 7** Temperature dependence of: **a** yield stress and **b** ultimate tensile stress

leading to the enhancement off 0.2%YSand UTS can be accounted for [12, 18, 19, 26].

#### 2.5.2 Effect of thermal expansion mismatch

The difference in CTE of the constituents of the composite solder may result in thermal stresses around reinforcement nano-sized particles which may induce plastic deformation in the matrix leading finally to the observed increase in the 0.2%YS and UTS [27, 28].

#### 2.5.3 Orowan strengthening

The interaction between dislocations and harden nano-sized particles resist the motion of the generating dislocations [29]. The accumulated dislocations on different boundaries in the matrix prevent further dislocation migration leading to strengthening of the material [27, 30, 31]. The result of this process on the yield stress as well the UTS of the material is expressed by Orowan strengthening mechanism. The contributions of various strengthening mechanisms to the yield strength of the composite solder were reported [14]. The observed decrease in the yield stress with increasing testing temperature is mainly due to the weakening effect of mismatch strain. This is because the non-coarsening ZnO-nano-sized particles have high degree of thermal stability, and thus, their Orowan strengthening isn't affected by the testing temperature.

#### 2.5.4 Adsorption of the nano-sized ZnO particles

During solidification of the melted plain solder, the presence of nano-sized ZnO particles leads to refinement. This may be rendered to the adsorption of ZnO particles on the surfaces of the solidified grains through the matrix. This behavior decreases the growth velocity of the IMCs. The proposed mechanism for the effect of nano-sized ZnO particles on refinement of the SnSb as well as the $Ag_3Sn$ IMCs can be summarized as follows: The mechanically dispersed nano-sized ZnO particles in the molten SSA plain solder are clinging to the large-sized β-Sn, SnSb as well as the $Ag_3Sn$ just as spheres cling to a plane. Accordingly the adsorption of such nano-sized surface active material can decrease the surface energy of these IMC particles [23–25],which led to the observed decrease of these IMC crystallites as presented in Fig. 4b, d. From this standpoint, the obtained microstructure of the composite solder reflects itself and improves the tensile response of the composite solder.

### 2.6 Stress exponent

Figure 8 shows the double-logarithmic relation between UTS and $\dot{\varepsilon}$ (strain rate) for both LFS alloys at different testing temperatures. Linear relationship is observed; which implies the power law relation:

$$\varepsilon = C\sigma^n \quad (1)$$

where σ is UTS, n is the stress exponent, and C is a material constant.

These n values were calculated from slopes of the straight lines of the double-logarithmic relation obtained in Fig. 8.

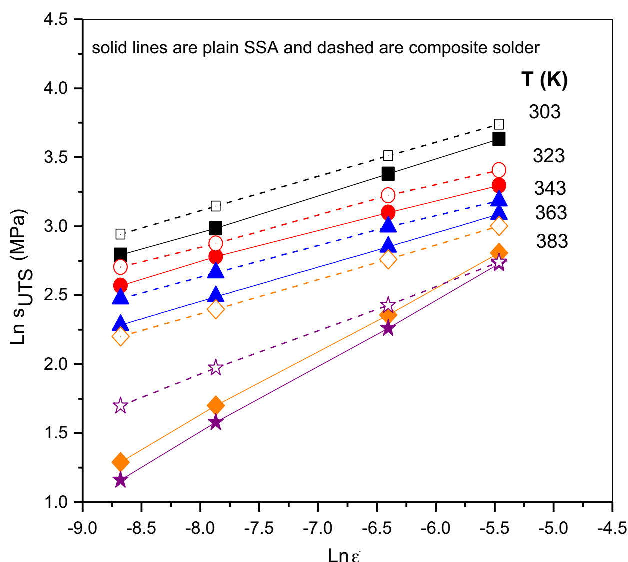


**Fig. 8** Relation between ln $\sigma_{UTS}$ and ln $\varepsilon^{\cdot}$ (strain rate) at different testing temperatures

Figure 9 illustrates the variation of n with the testing temperature for both the plain and composite LFS alloys. This figure showed that, n decreases with increasing testing temperature from ~4.6 to ~3.9 for the composite solder while it decreases from ~4.1 to 2.1 for the plain solder in the applied temperature range. This decrease of n could be attributed to the instability of the microstructure of the solders under investigation at high temperatures. It should be noted that the value of n decreases rapidly at temperatures higher than 353 K (0.7 $T_m$) for both plain and composite solder alloys. Also it is also noted that the composite solder is higher

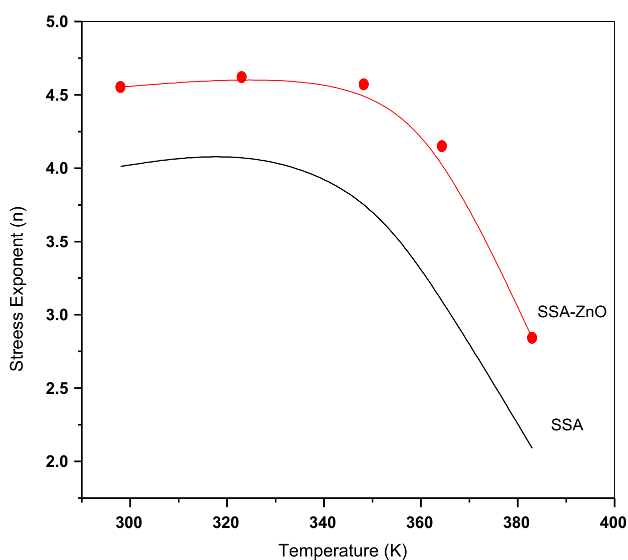


**Fig. 9** Relation between stress exponent and testing temperature

resistant for necking since it has higher values of n which means higher thermal stability.

## 2.7 Activation energy

For LFS alloys, plastic deformation is predominated by different mechanisms at $(T/T_m) \geq 0.5$ that are related to different values of stress exponent n and energy of activation Q. Generally, the strain rate $\varepsilon^{\cdot}$ is related to the testing temperature T, the ultimate tensile stress σ, the stress exponent n and energy of activation (Q) by Norton–Dorn equation [20]

$$\varepsilon^{\cdot} = A\sigma^n \exp\left(-Q/RT\right) \quad (2)$$

where A is that a material constant, R is the universal gas constant (R = 8.314 J/mol K). The energy of activation Q of the investigated solder was obtained from experimental results relating ln$\sigma_{UTS}$ and 1000/T (Fig. 10). It is well-known that values of n and Q are frequently used to determine the mechanisms dominant the deformation method.

As presented in Fig. 9, stress exponents values are reduced with increasing temperature within the used testing temperature range. Moreover, n values of the SSA composite solder exhibited higher values than that of the plain solder alloy, since the β-Sn grains are finer making composite solder to be harder. These results are quite in agreement with those reported for some SAC composite solder alloys [26, 32–34]. However, the higher the tress exponent is, the higher the strengthening result of alloy matrix. It's usually better-known that values of n are seven

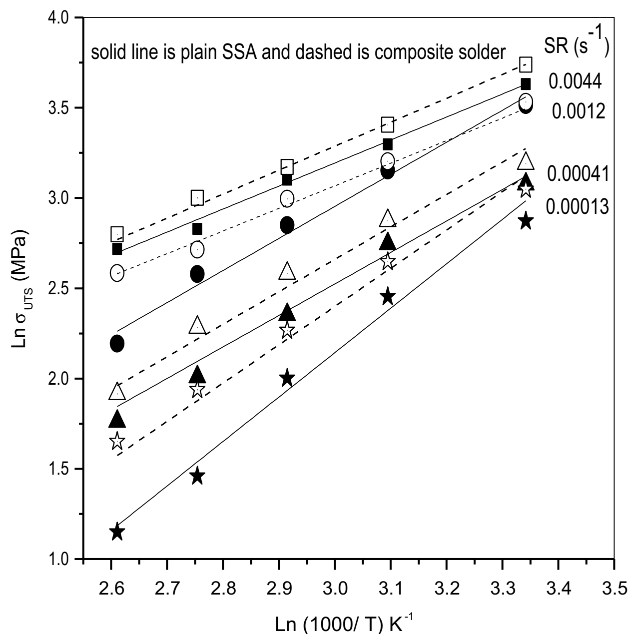


**Fig. 10** ln $\sigma_{UTS}$ and 1000/T at different strain rates for both the plain and composite solder alloys

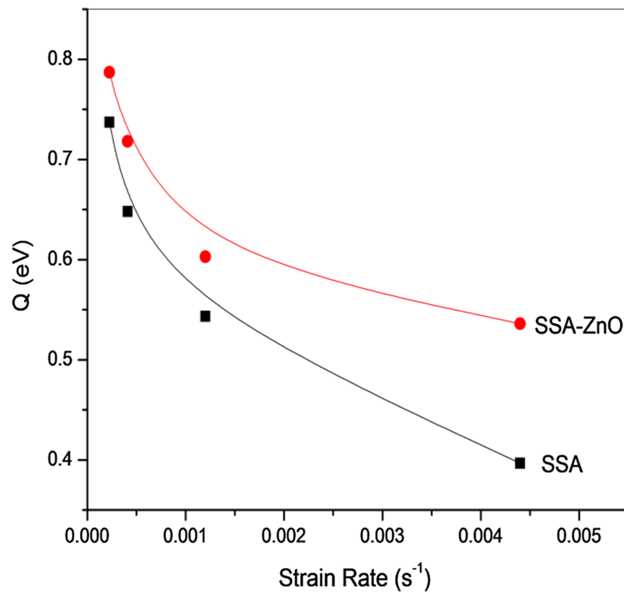


**Fig. 11** Strain rate dependence of the activation energy for both the plain and composite solder alloys

for the dispersion strong alloys, three for primary solid solution alloys and a two of for grain boundary sliding kind alloys [35].

The variation of activation energy with strain rate is illustrated in Fig. 11. It was found to decrease with increasing the strain rate. In the used range of strain rates, Q of composite solder decreased from ~0.8 to 0.5 eV, whereas for the plain solder it slashed from ~0.7 to 0.4 eV, respectively. The present results are about to the activation energies for dislocation climb power-assisted by vacancy diffusion through the dislocation core within the Sn-based solder alloys [18]. On the opposite hand, these results are not up to the energy of activation of the lattice self-diffusion of Sn (1.04–1.35 eV) [36]. It has been reported conjointly that the dislocation climb through the obstacles of Sn–5Sb and Sn–5Sb–3.5Ag, could result in values of n = 5.4 and Q = 0.56 eV, at low stress levels [37]. However, these values are in agreement therewith of n and Q obtained for the solder alloys within the present study, and are about to that reported for the pipe-diffusion-controlled creep of tin (0.42–0.65 eV) [38, 39], indicating that the plastic deformation of this alloys is ruled by the IMCs response. Besides, it ought to be stressed here that the determined variations within the n and Q values didn't have an effect on the rate controlling mechanism for this solder alloys.

## 3 Conclusion

In the present work, the effect of reinforcing ZnO particles on the microstructure, thermal behavior and corresponding tensile properties of Sn–5wt%Sb–1.5wt%Ag (SSA) LFS was investigated. The most important findings are:

- Microstructure investigations revealed that addition of nano- sized ZnO particles to SSA LFS inhibited the grain growth of the grains of the β-n matrix and refined the IMCs (SnSb and $Ag_3Sn$)
- The UTS and 0.2% YS became higher after addition of nano-sized ZnO particles. In addition, they increased with increasing strain rate and/or decreasing temperature.
- The adsorption of the harden ZnOnano-sized particles is considered as the main strengthening mechanism taking place in the composite solder.
- Consistent with the obtained values of stress exponents and energy of activation, it's planned that the dominant deformation mechanism in each LFS alloys is rate dominant mechanism mainly dislocation climb.
- From the experimental results it is supposed that SSA-ZnOnano-sized particles are proved to be a useful alternative to Pb containing solder system.

## References

1. A.R. Geranmayeh, G. Nayyeri, R. Mahmudi, Mater. Sci. Eng. A **547**, 110–119 (2012)
2. A.B. El Basaty, A.M. Deghady, E.A. Eid, Mater. Sci. Eng. A **701**, 245–253 (2017)
3. M. Abtewa, G. Selvaduray, Mater. Sci. Eng. R **27**, 95–141 (2000) **288–290**
4. K.J. Puttlitz, K.A. Stalter, *Handbook of Lead-Free Solder Technology for Microelectronic Assemblies* (Marcel Dekker, Inc, New York, 2004), pp. 292–294
5. K. Suganuma, K.S. Kim, J. Mater. Sci. **18**, 121–127 (2007)
6. A.A. El-Daly, Y. Swilem, A.E. Hammad, J. Alloys Compd. **471**, 98–104 (2009)
7. A.K. Gain, Y.C. Chan, W.K.C. Yung, Microelectron. Reliab. **5**, 975–984 (2011)
8. L.C. Tsao, S.Y. Chang, C.I. Lee, W.H. Sun, C.H. Huang, Mter. Des. **31**, 4831–4835 (2010) 10 )
9. S. Chellvarajoo, M.Z. Abdullah, Mater. Des. **90**, 499–507 (2015)
10. Y. Tang, G.Y. Li, Y.C. Pan, J. Alloys Compds. **554**, 195–203 (2013)
11. M. Kangooe, R. Mahmudi, A.R. Geranmayeh, J. Electron. Mater. **39**, 2 (2010)
12. E.A. Eid, A.N. Fouda, M. El-Shazly, Duraia, Mater. Sci. Eng. A **657**, 104–114 (2016)
13. R.K. Shiue, L.W. Tsay, C.L. Lin, J.L. Ou, J. Mater. Sci. **38**, 1269 (2003)
14. A.N. Fouda, E.A. Eid, Mater. Sci. Eng. A **632**, 82–87 (2015)
15. F. Gao, T. Takemoto, H. Nishikawa, Mater. Sci. Eng. **A420**, 39–46 (2006)

16. S. Ji, Z. Fan, Metall. Mater. Trans. A **33A**, 3511–3520 (2002)
17. G.S. Al-Ganainy, A.A. El-Daly, A. Fawzy, N. Hussein, J. Mater. Sci. **28**, 13303–13312 (2017)
18. A. Fawzy, S.A. Fayek, M. Sobhy, E. Nassr, M.M. Mousa, G. Saad, Mater. Sci. Eng. A **603**, 1–10 (2014)
19. A. Fawzy, S.A. Fayek, M. Sobhy, E. Nassr, M.M. Mousa, G. Saad, J. Mater. Sci. **24**, 3210–3218 (2013)
20. P. Babaghorbani, S.M.L. Nai, M. Gupta, J. Mater. Sci. **20**, 571–576 (2009)
21. A.A. El-Daly, A.E. Hammad, G.S. Al-Ganainy, A.A. Ibrahiem, Mater. Des. **56**(–), 594–603 (1980) 2015)
22. M.F. Ashby, Surf. Sci. **31**, 498 (1972)
23. L.C. Tsao, S.Y. Chang, Mater. Des. **31**, 990 (2010)
24. D.Q. Yu, L. Wang, C.L. Wu, C.M.T. Law, J. Alloy Compd. **389**, 153 (2005)
25. L.C. Tsao, J. Alloy Compd. **509**, 2326 (2011)
26. A.A. El-Daly, T.A. Elmosalami, W.M. Desoky, M.G. El-Shaarawy, A.M. Abdraboh, Mater. Sci. Eng. A **618**, 389–397 (2014)
27. A.R. Geranmayeha, R. Mahmudi, M. Kangooie, Mater. Sci. Eng. **A528**, 3967–3972 (2011)
28. K. M. Kumar, V. Kripesh, A.A. Tay, J. Alloy Compd. **455**, 148–158 (2008)
29. F.A. Mirza, D.L. Chen, Materials **8**, 5138–5153 (2015)
30. X.L. Zhong, W.L.E. Wong, M. Gupta, Acta Mater. **55**, 6338–6344 (2007)
31. Khin, SandarTun, M. Gupta, Compos. Sci. Technol. **67**, 2657–2664 (2007)
32. J. Shen, Y.C. Chan, J. Alloy Compd. **477**, 552–559 (2009)
33. A.A. El-Daly, A. Fawzy, S.F. Mansour, M.J. Younis, Mater. Des. **55**, 837–845 (2014)
34. A.A. El Daly, A. Fawzy, S.F. Mansour, M.J. Younis, Mater. Sci. Eng. A **578**, 62–71 (2013)
35. S. Wiese, K.J. Wolter, Microelectron. Reliab. **47**, 223 (2007)
36. J. Rodney, McCabe, M.E. Fine, Metall. Mater. Trans. A **33**(5), 1531–1539 (2002)
37. R. Mahmudi, A.R. Geranmayeh, H. Noori, M. Shahabi, Mater. Sci. Eng. A **491**, 110–116 (2008)
38. S.M.L. Nai, J. Wei, M. Gupta, Thin Solid Films **504**, 401–404 (2006)
39. P. Liu, P. Yao, J. Liu, J. Electron. Mater. **37**(6), 874–879 (2008)